International Journal of Modern Nonlinear Theory and Application, 2026, 15(3), 90-103
https://www.scirp.org/journal/ijmnta
ISSN Online: 2167-9487
ISSN Print: 2167-9479

# Computational Thermo-Fluid Dynamic and Mass Transfer Simulation of Anodic Oxidation in Copper Refining by Arc Electrolysis Using COMSOL Multiphysics

**Jorge Manríquez-Fica[1], Mario Ávila-Muñoz[2]**

[1]Metallurgical Engineering Department, University of Santiago of Chile, Santiago, Chile
[2]Research Group 8 Sustainable Materials Science, Department of Materials, Textiles and Chemical Engineering, Ghent University, Ghent, Belgium
Email: jorge.manriquez@usach.cl, mario.avila@ugent.bey

**How to cite this paper:** Manríquez-Fica, J. and Ávila-Muñoz, M. (2026) Computational Thermo-Fluid Dynamic and Mass Transfer Simulation of Anodic Oxidation in Copper Refining by Arc Electrolysis Using COMSOL Multiphysics. *International Journal of Modern Nonlinear Theory and Application*, **15**, 90-103.
https://doi.org/10.4236/ijmnta.2026.153008

**Received:** June 25, 2026
**Accepted:** July 24, 2026
**Published:** July 27, 2026



## Abstract

Metals such as copper and iron are commonly refined through pyrometallurgical processes, where air serves as the oxidizing agent to remove impurities. The final traces of residual oxygen are typically eliminated by adding deoxidizers to the molten metal, producing inclusions that either float to the surface or become trapped during solidification. An alternative approach consists of supplying oxygen to molten copper via anodic oxidation of oxyanions present in the slag, while cathodic reduction occurs at the arc-slag interface, under conditions that favor oxide valence reduction and evaporation. This paper presents a mathematical formulation describing the physics of arc electrolysis, including the spatial and temporal evolution of electric current, fluid dynamics, heat transfer, and mass transport—particularly the transfer of oxidizing agents from arsenic to copper. A three-dimensional finite element model was developed in COMSOL Multiphysics to couple direct current conduction, fluid flow, heat transfer, and mass transport for oxygen transfer from slag to synthetic blister copper in a DC arc furnace. Thermal balance results indicated an arc temperature of 2067 K, which generates natural convection driven by temperature gradients that also produce concentration gradients. The effect is more pronounced in the slag near the heat source, where velocity reaches 6.75 $\times 10^{-7}$ m/s, compared with a maximum of 9.72 $\times 10^{-10}$ m/s in molten copper. Oxygen transport simulations showed that an initial homogeneous concentration of 2446 mol/m$^3$ evolves after 2000 seconds into a profile ranging from 1840 mol/m$^3$ at the slag-gas interface to 759 mol/m$^3$ at the metal-slag interface, where electrochemical oxidation occurs. In copper, oxygen—initially absent—

develops a profile with a maximum of 291 mol/m$^3$ at the metal-slag interface and 184 mol/m$^3$ at the crucible bottom.

## Keywords

Arc Electrolysis, Pyro Refining, Modeling, Simulation, Slag, Blister Copper

## 1. Introduction

The conventional route for refining copper and other non-ferrous metals is pyrometallurgical processing. Impurity levels directly affect copper pricing, with penalties ranging from 0.9 to 4.1 US$/lb. The standard equipment employed is the rotary pyrorefining furnace, which operates in two sequential steps: oxidation-complexing (Equation (1)) and reduction (Equation (2)).

$$S + O_{2(gas)} = SO_{2(gas)} \quad (1)$$

$$\underline{C} + \underline{O} = CO_{2(gas)} \quad (2)$$

In this process, oxygen content represents the main variable. The classic method of control involves the use of solid-state cells to measure oxygen levels, followed by verification with Leco analysis in the chemical laboratory.

Refining by arc electrolysis is considered an alternative means of removing impurities from molten copper without introducing deoxidizing agents. This electrochemical method replaces the chemical reactions involved in oxidation and reduction with electrochemical reactions.

In the electrochemical technique, the gaseous chemical oxidant can be replaced by electrons, which enter the process through inert and/or reactive electrodes.

In this work, we study the dynamic behavior of anodic oxidation of oxyanions as the source of oxidizing agents for impurities in blister copper, using COMSOL Multiphysics 6.0.

## 2. Theoretical Basis

### 2.1. Anodic Oxidation

The slag consists of oxides such as CaO, $SiO_2$, and $Cu_2O$. According to the ionic theory of metallurgical slags [1], these oxides can be considered ionized. The oxidation of ionic oxygen in the slag to oxygen dissolved in copper occurs as follows:

$$O^{2-} \rightarrow 2e^- + \underline{O} \quad (3)$$

If the chemical removal of non-metallic impurities such as sulfur from molten copper is considered, the following possible reaction occurs (Equation (4)):

$$S + 2\underline{O} = SO_{2(gas)} \quad (4)$$

It is evident that no external gaseous oxygen has been supplied. Oxygen introduced into copper can also react with other impurities (Me) to form oxides ($Me_xO_y$), which are insoluble in blister copper and fixed in the slag. Oxidation proceeds

according to Equation (5):

$$x\underline{Me} + y\underline{O} \rightarrow Me_xO_{y(slag)} \quad (5)$$

The oxide in the slag dissociates according to Equation (6).

$$Me_xO_{y(slag)} \rightarrow x\,Me^{2+} + y\,O^{2-} \quad (6)$$

The oxyanion migrates to the anode and undergoes oxidation according to Equation (3), while the cation migrates to the cathode, where it may either reduce its valence (Equation (7)) or revert to its elemental state (Equation (8)):

$$Me^{2+} \rightarrow Me^{+} + e^{-} \quad (7)$$

$$Me^{2+} \rightarrow Me^{0} + 2e^{-} \quad (8)$$

Additionally, when an arc is generated, the impact zone on the slag surface forms a "beam cathode", where conditions favor valence reduction and metal evaporation.

## 2.2. Physical System

The arc electrolysis furnace consists of a cylindrical crucible (Figure 1).

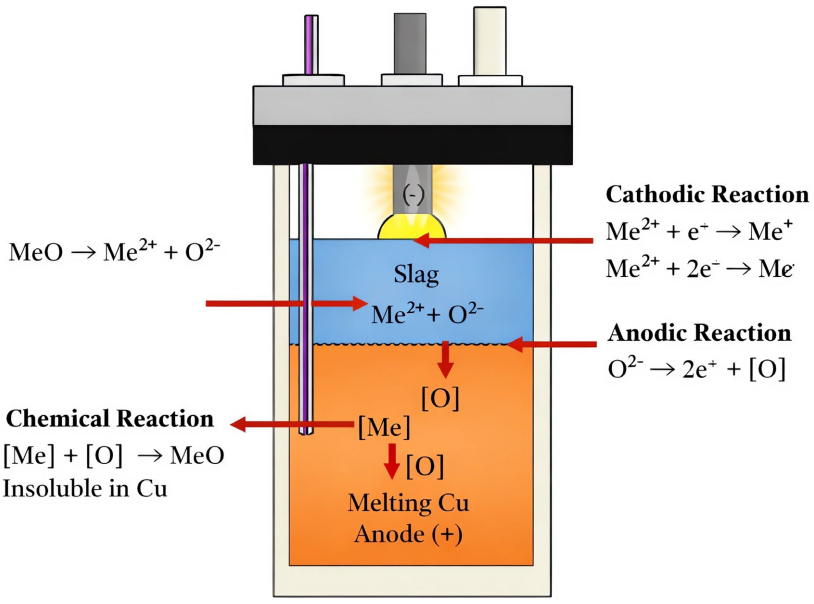


Figure 1. Arc electrolysis furnace scheme.

The crucible, made of mullite, is housed in a furnace lined with silica refractory bricks and heated by silicon carbide electrodes. A single graphite electrode enters through the top seal. Copper blister and slag are loaded from above prior to heating and sealing. Once melted at 1500 K, the electrode is positioned 1 mm above the slag bath to generate the arc [2].

Understanding DC arc behavior is crucial for impurity removal, particularly for volatile species. This study investigates the dynamic oxidation behavior of oxygen anions as oxidizing agents for impurities in blister copper.

### 2.3. Conductive Medium DC (Direct Current)

To model the influence of electrolysis on copper refining, the DC conductive medium is employed. This framework represents how electric current flows through the system and couples with the governing equations of mass and energy transport.

The conductive medium is characterized by its electrical conductivity ($\sigma$) and a stable current ($I$). The current density ($J$) is related to the electric field ($E$) by the expression:

$$J = \sigma \cdot E \tag{9}$$

When an external current ($J_0$) is included, the total field becomes:

$$J_{tot} = J + J_0 = \sigma \cdot E + J_0 \tag{10}$$

Combining the continuity equation.

$$\nabla \cdot J_{tot} = 0 \tag{11}$$

With the definition of electric potential.

$$E = \nabla \cdot V = 0 \tag{12}$$

Yields.

$$-\nabla \cdot (\sigma \nabla \cdot V) = Q = 0 \tag{13}$$

where $Q$ is the source term.

The graphite anode was assigned a fixed potential of 20 V, while the bottom of the crucible, acting as the cathode, was grounded at 0 V. The electrical conductivities of the materials were explicitly parameterized to ensure accurate representation of the electric field distribution.

The arc region was modeled with a height of 2.25 mm, where Joule heating was applied as a volumetric source $Q$. Radiative losses were included using an emissivity of 0.5 and the Stefan-Boltzmann constant $\sigma_{SB} = 5.67 \times 10^{-8}$ W/(m$^2$·K$^4$).

### 2.4. Navier-Stokes Equation

The fluid flow in the COMSOL model was treated as laminar, with turbulence effects neglected due to the relatively small characteristic dimensions and moderate Reynolds numbers. The density of both slag and molten copper was assumed to be temperature-independent, and buoyancy body forces were introduced in the copper and slag domains through the expressions $\beta_{\mathrm{Cu}} * g * (T - T_{\mathrm{furnace}})$ and $\beta_{\mathrm{Slag}} * g * (T - T_{\mathrm{furnace}})$, where $\beta$ denotes the buoyancy coefficient (K$^{-1}$). This formulation enabled the incorporation of natural convection by coupling the thermal field with the momentum equations, ensuring that temperature differences within the system generated the corresponding buoyancy-driven flow.

The Navier-Stokes equations, which govern fluid motion in the slag and molten copper under natural convection conditions, describe viscous, incompressible fluid flow and the associated phenomena of mass and momentum transport [3]:

$$\frac{\partial u}{\partial t} + \rho u \cdot \nabla u + \nabla p = \nabla \cdot \eta \left( \nabla u + (\nabla u)^{\mathrm{T}} \right) + F \tag{14}$$

And the continuity equation.

$$\left(\nabla \cdot u\right) = 0 \tag{15}$$

### 2.5. Heat Transfer Equation

The heat transfer equation, which accounts for conduction, convection, and radiation, is represented by Equation (16).

$$\frac{\partial \rho C_p T}{\partial t} + \rho C_p u \nabla T = \nabla\left(k \nabla T\right) + Q \tag{16}$$

Equation (16) includes the following quantities: heat flux by convection ($\rho \cdot C_p \cdot u \cdot \nabla T$), heat flux by conduction ($\nabla \cdot (k \nabla T)$), heat source ($Q$), thermal conductivity ($k$) and specific heat capacity at constant pressure ($C_p$).

Natural convection was incorporated by coupling the momentum equations with the thermal field, where local variations in temperature generated gradients that drove fluid motion. This approach allowed the model to capture the essential features of buoyancy-driven flow.

### 2.6. Mass Transfer Equation

The mass transport equation, which models the diffusion and convection of chemical species—specifically oxygen in this case—is represented by Equation (17):

$$\frac{\partial c_i}{\partial t} + \rho u \nabla c_i = \nabla\left(D_i \nabla c_i\right) + R_i \tag{17}$$

Equation (17) includes the following quantities: concentration of species $i$ ($c_i$), diffusion coefficient ($D_i$), reaction rate expression for species $i$ ($R_i$), velocity vector ($u$).

At the slag-metal interface, a boundary condition was defined to represent the electrochemical oxygen transfer according to Faraday's law. Where $J$ is the local current density obtained from the electric currents module. In the present model, this boundary condition was assumed to be controlled exclusively by the current density distribution, without the inclusion of explicit interfacial kinetic parameters. A Faradaic efficiency of 100% was defined, implying that the total electrical current contributes directly to the electrochemical oxidation of oxyanions in the slag and the subsequent oxygen transfer into the copper phase. This assumption ensures a consistent coupling between the electric currents and species transport modules, while acknowledging that interfacial kinetics could be incorporated in future refinements of the model.

## 3. System Modelation

### 3.1. Geometry

The modeled geometry (**Figure 2**) consists of a cylindrical crucible (10 cm in height, 2.5 cm in radius) containing molten blister copper with a height of 5 cm, which serves as the cathode (−). Above this, a slag layer of 2.25 cm in height is

placed. The arc is modeled with a height of 2.25 mm to account for bath agitation caused by thermal effects, thereby ensuring that the arc is always maintained with a minimum of 1 mm. The graphite electrode, which serves as the anode (+), has a diameter of 6.6 mm and a length of 4 cm.

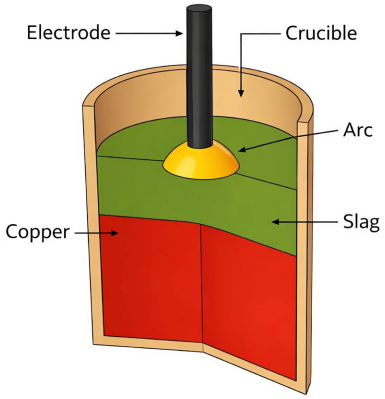


**Figure 2.** Geometry used in the modelling. Domains: electrode, arc, slag, copper and crucible.

## 3.2. Meshing

The mesh used for the computational fluid dynamics simulation is shown in **Figure 3**.

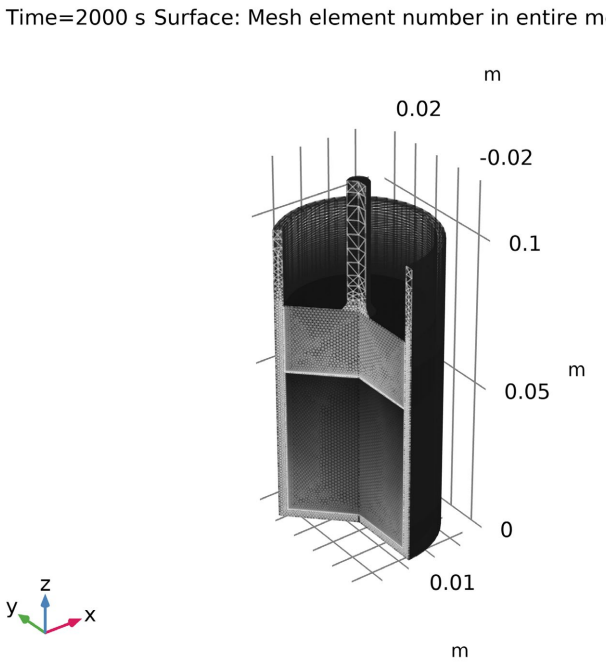


**Figure 3.** Mesh used for the computational electrolysis arc simulation.

The mesh was refined at the walls, as well as at the slag-metal and arc-slag interfaces. The complete mesh consists of 6290 elements, with a minimum quality of 0.4412 and an average quality of 0.8223.

A mesh sensitivity study was conducted to verify numerical stability and mesh independence. Simulations with progressively finer meshes were performed, monitoring the maximum arc temperature and the interfacial oxygen flux at the slag-copper boundary. Between the two finest meshes (6290 and 9988 elements), the maximum arc temperature varied from 2067.1 K to 2071.2 K (relative difference 0.2%), while the interfacial oxygen flux changed from $9.08 \times 10^{-3}$ to $8.99 \times 10^{-3}$ mol/m²·s (relative difference 0.99%). These small variations confirm mesh independence of the solution.

### 3.3. Domains

The system comprises five domains, 19 edges, and 15 points. The physical properties of the subdomains are presented in Table 1.

Table 1. Physical properties of the domains considered in the COMSOL model.

| Domain | Density (kg/m³) | Thermal conductivity (W/(m·K)) | Specific heat (J/(kg·K)) | Viscosity (Pa·s) | Electrical conductivity (S/m) | Diffusivity (m²/s) | Buoyancy coefficient ($K^{-1}$) |
|---|---|---|---|---|---|---|---|
| Copper | 7600 | 400 | 500 | 0.005 | $1.0 \times 10^{8}$ | $1.0 \times 10^{-6}$ | $1.0 \times 10^{-6}$ |
| Slag | 3500 | 3 | 1200 | 0.2 | 100 | $1.0 \times 10^{-7}$ | $1.0 \times 10^{-5}$ |
| Arc | 10 | 50 | 10 | - | 30 | - | - |
| Graphite | 2000 | 30 | 2000 | - | $1.0 \times 10^{4}$ | - | - |
| Crucible (MgO) | 3000 | 3 | 1900 | - | - | - | - |

### 3.4. Boundary and Initial Conditions

Table 2 summarizes the boundary and initial conditions applied in the computational model to solve the coupled equations of momentum, heat, and mass transfer.

Table 2. Boundary and initial conditions for momentum, heat, and mass transfer.

| Condition type | Equation/Value | Description | Application domain |
|---|---|---|---|
| Momentum Wall condition | $u = 0$ | No-slip condition to capture shear stresses. | Crucible walls |
| Momentum Natural convection | Navier-Stokes (Equation (12) and (13)) | Buoyancy-driven flow induced by temperature gradients. | Slag and copper domains |
| Momentum Symmetry planes | $n \cdot \nabla u = 0$ | Simplifies computation by symmetry assumption. | Converter symmetry planes |
| Heat Initial furnace temperature | $T_0 = 1500$ K | Starting condition for thermal field. | Entire system |

**Continued**

| | | | |
|---|---|---|---|
| Heat Radiative losses | $\varepsilon = 0.5$ | Radiation modeled with Stefan-Boltzmann law. | Crucible external walls |
| Heat Adiabatic isolation | $n \cdot (-k\nabla T) = 0$ | No heat flux across insulated boundaries. | Crucible lateral walls |
| Mass Initial oxygen in slag | $CO_2 = 2446$ mol/m$^3$ | Derived from stoichiometric $Cu_2O$ content. | Slag domain |
| Mass Initial oxygen in copper | $CO_2 = 0$ mol/m$^3$ | Copper assumed oxygen-free at start. | Copper domain |
| Mass Electrochemical flux | Equation (16) $N_O \propto J_z$ | Oxygen transfer proportional to current density. | Slag-metal interface |
| Mass-Symmetry planes | $n \cdot \nabla c_i = 0$ | Zero gradient condition to reduce computational cost. | Converter symmetry planes |
| Mass-No flux (isolation) | $n \cdot (-D_i \nabla c_i) = 0$ | Prevents species transfer across external boundaries. | Crucible walls |

These conditions define the physical constraints of the system, including no-slip walls, symmetry planes, radiative and adiabatic boundaries, as well as the initial thermal and chemical states of slag and blister copper. By explicitly specifying these parameters, the model ensures consistency across domains and provides the basis for capturing the electrochemical transfer of oxygen under arc electrolysis conditions.

The flux of oxygen transferred from the slag to the blister copper by anodic oxidation is proportional to the electrical current passing through the molten electrolyte, as expressed in Equation (18).

$$N_O\left[\frac{\text{mol}}{\text{m}^2 \cdot \text{s}}\right] = V_{slag}\left[\text{m}^3\right] \times c_O\left[\frac{\text{mol}}{\text{m}^3}\right] \times \frac{1}{z_O F\left[\text{C}\right]} \times J_z\left[\frac{\text{A}}{\text{m}^2}\right] \tag{18}$$

$c_0$ denotes the concentration of oxygen in the slag, obtained from the mass transport equation, while $J_z$ represents the total current density, derived from the coupling with the DC conductive medium equation for the $z$ component of the current density.

## 4. Results and Discussion

The field profiles of voltage, current density, velocity, temperature, and oxygen concentration in both slag and blister copper after 2000 seconds of simulation are presented below. These represent a subset of the extensive data generated by the software, which also includes molar oxygen fluxes (in slag and copper), pressure distributions, heat fluxes, and heat generation due to the Joule effect, among other parameters.

The following Figure 4(a) illustrates the potential field, which reaches its maximum at the upper end of the electrode where 20 volts are applied, and its minimum at the ground connection located at the bottom of the crucible, corresponding to 0 volts. The predicted arc temperature of approximately 2067 K is consistent with values reported in plasma arc simulations, which typically range between 2000 - 2200 K [4].

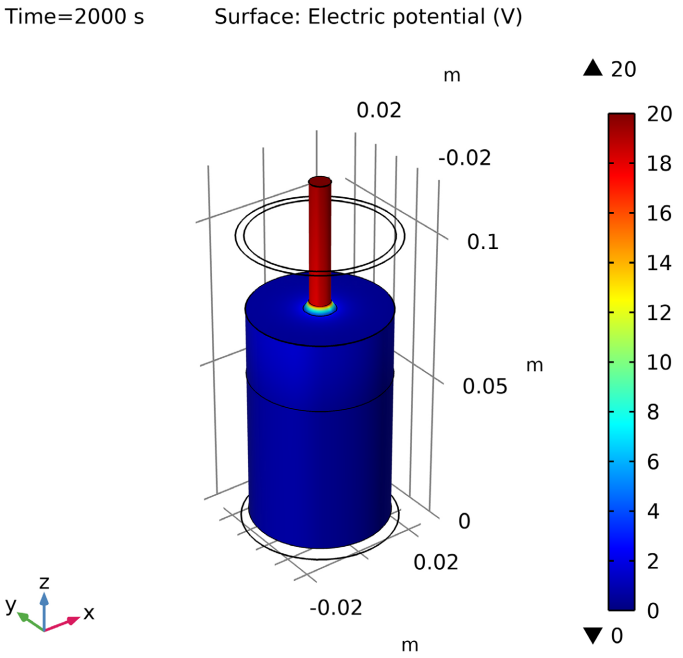


(a)

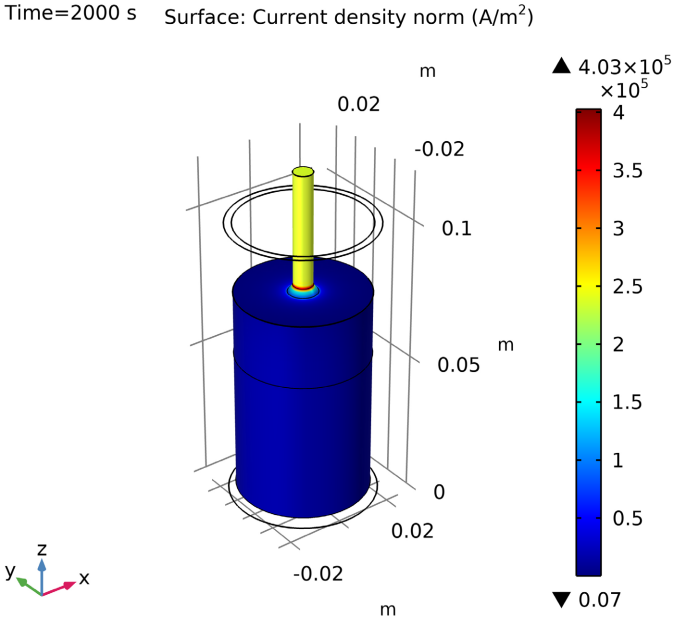


(b)

Figure 4. Field of potential, V, in the refining system by arc electrolysis (a), field of density current, A/m², in the refining system by arc electrolysis. (b).

Figure 4(b) presents the current density distribution, showing values of 346,960 A/m$^2$ at the electrode-gas interface, 65,214 A/m$^2$ at the gas-slag interface, and 4606.7 A/m$^2$ at the copper-slag interface. This current density corresponds to the equivalent oxygen mass transported from the slag to the blister copper through the anodic oxidation of oxyanions.

The pronounced difference between the very high current density at the electrode-gas interface (346,960 A/m$^2$) and the much lower value at the copper-slag interface (4606.7 A/m$^2$) is explained by the voltage drop across the system and the resulting distribution of the electric field.

At the electrode-gas interface, the full applied potential of 20 V is concentrated at the electrode tip over a small contact area. This sharp potential gradient produces an intense electric field and, consequently, a very high current density. This region represents the maximum electron injection zone.

As the current passes through the arc and enters the slag, a significant portion of the applied voltage is consumed due to the slag's relatively high electrical resistance. The electric field weakens, and the current density decreases to intermediate values (65,214 A/m$^2$). In this region, electrochemical oxidation of oxyanions begins to occur.

At the slag-copper interface, the remaining potential is already much lower. Although copper is a highly conductive medium, the reduced voltage available at this boundary limits the driving force for charge transfer. The current therefore disperses more efficiently throughout the metallic phase, further attenuating the local electric field. This explains why the current density drops significantly at the slag-copper interface, while still remaining sufficient to sustain the electrochemical transfer of oxygen into the copper.

The observed current density distribution, governed by the progressive voltage drop across the gas, slag, and copper layers, is consistent with ranges reported in DC field-enhanced smelting studies [5].

Likewise, the maximum current density at the electrode-gas interface (346,960 A/m$^2$) falls within the order of magnitude observed in experimental arc electrolysis studies [6].

The next Figure 5(a) illustrates the velocity field (arrows) determined by the Navier-Stokes equations in both the slag and molten copper. This motion is driven by natural convection, arising from temperature gradients that subsequently generate concentration gradients. The effect is more pronounced in the slag near the heat source, where velocity reaches $6.75 \times 10^{-7}$ m/s. In copper, natural convection is weaker, with maximum velocities on the order of $9.72 \times 10^{-10}$ m/s. Both velocity profiles (slag and copper) exhibit a vortex pattern, characterized by ascending flow lines at the center of the crucible and descending lines along the walls.

The subsequent Figure 5(b) presents the thermal profile, where the arc reaches a high temperature of approximately 2067.1 K due to Joule heating—the heat generated by the passage of electric current and the electrical resistance of the arc—reaching a maximum of $4.56 \times 10^9$ W/m$^3$. The temperature decreases gradually

with distance from the arc, eventually returning to the initial furnace temperature of 1500 K across nearly half of the slag and throughout the copper.

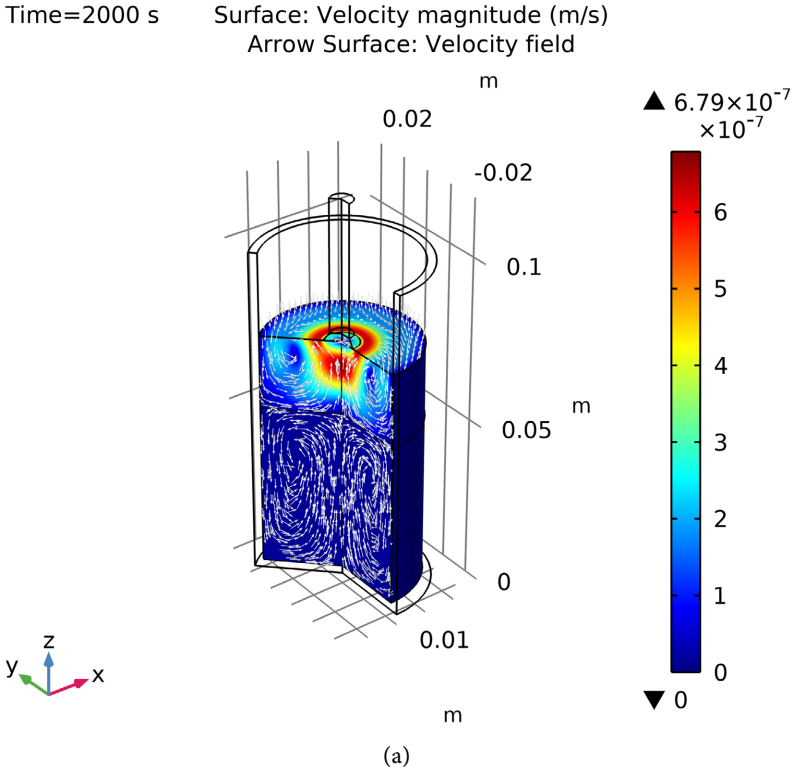


(a)

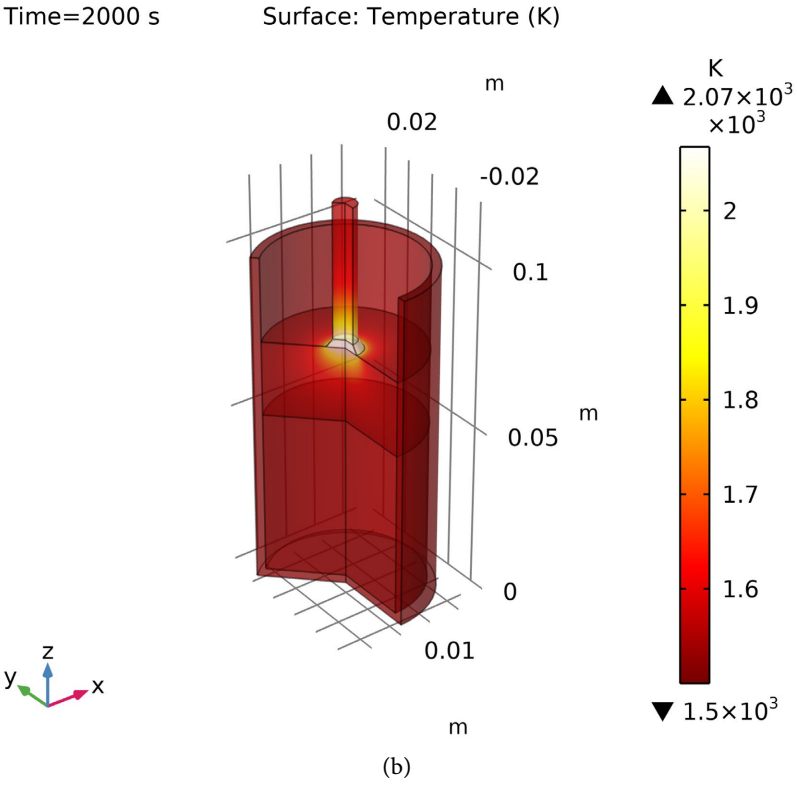


(b)

**Figure 5.** Velocity field in Slag and Blister Copper, m/s (a), Temperature Profile, K (b).

The disparity in velocity magnitudes between slag and copper arises from their distinct physical properties and thermal responses. In the slag, lower density and reduced thermal conductivity allow temperature gradients to persist, generating buoyancy forces that drive natural convection. This results in higher velocities, reaching $6.75 \times 10^{-7}$ m/s, and a pronounced vortex pattern. In contrast, molten copper is denser and exhibits much higher thermal conductivity, which rapidly dissipates temperature gradients. Consequently, buoyancy-driven motion is weaker, with maximum velocities of only $9.72 \times 10^{-10}$ m/s.

Similarly, the temperature distribution reflects the contrasting thermal behavior of both media. The slag absorbs heat directly from the arc, reaching localized peaks of approximately 2067 K, while its low conductivity confines the heat near the source. Copper, however, efficiently conducts heat, smoothing out gradients and maintaining temperatures closer to the initial furnace value of 1500 K. This explains why Joule heating strongly affects the slag domain but produces only moderate thermal variations in the copper. The predicted arc temperature of approximately 2067 K is consistent with values reported in plasma arc simulations, typically between 2000 - 2200 K.

The initial oxygen concentration in the slag is 2446 mol/m$^3$. As shown in Figure 6(a), after 2000 seconds of simulation this develops into a profile ranging from a maximum of 1840 mol/m$^3$ at the slag-gas interface to a minimum of 759 mol/m$^3$ at the slag-metal interface, where anodic oxidation of the oxyanion occurs.

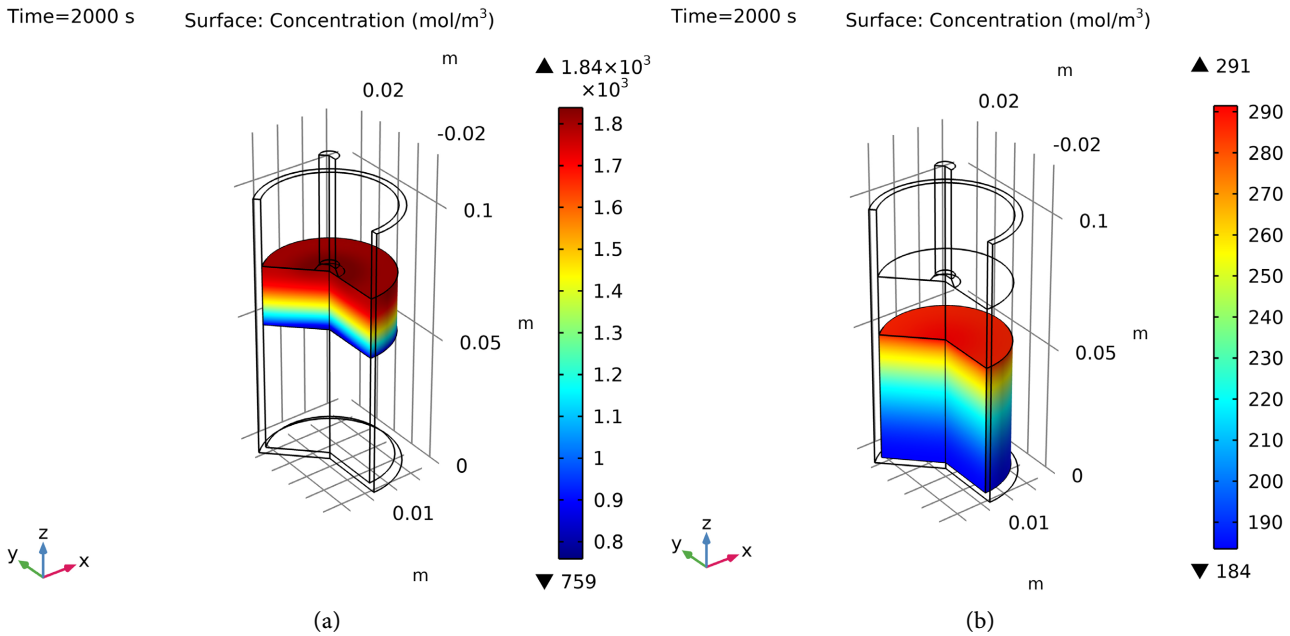


Figure 6. Profile concentration of oxygen in slag, mol/m$^3$ (a), profile concentration of oxygen in blister copper, mol/m$^3$ (b).

In copper, the initial oxygen concentration is 0 mol/m$^3$. Figure 6(b) shows that after 2000 seconds a profile emerges, with a maximum of 291 mol/m$^3$ at the slag-copper interface, where oxygen is electrochemically transferred from the slag. From this interface, oxygen is transported by diffusion and natural convection

toward the bottom of the crucible, where its concentration reaches 184 mol/m$^3$.

The average calculated oxygen fluxes in slag and copper were $4.36 \times 10^{-3}$ mol/m$^2$·s and $4.13 \times 10^{-3}$ mol/m$^2$·s, respectively. These values were obtained by performing a volumetric integration of the flux fields at 2000 seconds of simulation time. They are consistent with values reported for oxygen transfer in molten copper systems [7]. This agreement confirms that the simulated fields are physically plausible and fall within ranges documented in the literature, thereby reinforcing the reliability of the computational model.

## 5. Conclusions

The simulation results indicate an arc temperature of 2067 K, which induces fluid motion through natural convection. These convective currents are generated by temperature gradients that, in turn, produce concentration gradients. In the slag, the maximum velocity reaches $6.75 \times 10^{-7}$ m/s, while in molten copper the velocity is significantly lower, on the order of $9.72 \times 10^{-10}$ m/s.

After 2000 s of simulation, the oxygen concentration in the slag decreases from the initial 2446 mol/m$^3$ to a maximum of 1840 mol/m$^3$ at the slag-gas interface and a minimum of 759 mol/m$^3$ at the slag-metal interface, where anodic oxidation of the oxyanion occurs. In copper, oxygen concentration increases from zero to 291 mol/m$^3$ at the slag-copper interface, consistent with electrochemical transfer, and further diffuses to 184 mol/m$^3$ at the bottom of the crucible.

## Acknowledgements

The authors express their gratitude to the DICYT (050614MF) of the University of Santiago, Chile.

The authors express their gratitude to the Project 155LD of the University of Santiago, Chile.

The authors express their gratitude to the Society for Technological Development (SDT-USACH, Ltd.).

## Conflicts of Interest

The authors declare no conflicts of interest regarding the publication of this paper.

## References

[1] Gaskell, D.R. (1997) Structural Aspects of Slags. *Proceedings of the 5th International Conference on Molten Slags, Fluxes, and Salts '97*, Sydney, 5-8 June 1997, 11-26.

[2] Manríquez, J. (2022), Electrorefinación de cobre a alta temperatura. Disclosure G-0275, Dirección de Gestión Tecnológica de la Universidad de Santiago (DGT-USACH).

[3] COMSOL, Inc. (2022) COMSOL Multiphysics 6.0. License No. 2102699.

[4] Shelley, T.R. and Charles, J.A. (1974) Arc Electrolysis of Ferruginous Tin-Containing Melts: Pilot-Plant Experiments. *Transactions of the Institute of Mining & Metallurgy*, **83**, C18-C24.

[5] Powell, A. and Dussault, D. (2003) Scaling Laws and Instabilities in Electric Field-enhanced Smelting and Refining of Steel. *Scandinavian Journal of Metallurgy*, **32**, 33-36. https://doi.org/10.1034/j.1600-0692.2003.20549.x

[6] Reynolds, Q.G., Jones, R.T. and Reddy, B.D. (2010) Mathematical and Computational Modelling of the Dynamic Behaviour of Direct Current Plasma Arcs. *The Journal of the Southern African Institute of Mining and Metallurgy*, **110**, 789-801.

[7] Fukunaka, Y., Nishikawa, K., Sohn, H.S. and Asaki, Z. (1991) Desulfurization Kinetics of Molten Copper by Gas Bubbling. *Metallurgical Transactions B*, **22**, 5-11. https://doi.org/10.1007/bf02672520